Magnetic properties and magnetocaloric effects of $Tm_{1-x}Er_xCuAl$ ($x = 0.25$, 0.5, and 0.75) compounds

Hao Sun(孙浩)[1,2], Junfeng Wang(王俊峰)[2], Lu Tian(田路)[2], Jianjian Gong(巩建建)[1,2], Zhaojun Mo(莫兆军)[2,†], Jun Shen(沈俊)[3], and Baogen Shen(沈保根)[1,‡]

[1] *School of Rare Earths, University of Science and Technology of China, Hefei* 230026, *China*
[2] *Ganjiang Innovation Academy, Chinese Academy of Sciences, Ganzhou* 341000, *China*
[3] *Key Laboratory of Cryogenics, Technical Institute of Physics and Chemistry, Chinese Academy of Sciences, Beijing* 100190, *China*

(Received 14 June 2022; revised manuscript received 9 August 2022; accepted manuscript online 16 August 2022)

We investigate the structural, magnetic, and magnetocaloric effects (MCE) of $Tm_{1-x}Er_xCuAl$ ($x = 0.25$, 0.5, and 0.75) compounds. The compounds undergo a second-order phase transition originating from the ferromagnetic to paramagnetic transition around 3.2 K, 5 K, and 6 K, respectively. The maximum magnetic entropy changes ($-\Delta S_M^{max}$) of $Tm_{1-x}Er_xCuAl$ ($x = 0.25$, 0.5, and 0.75) are 17.1 J·kg^{-1}·K^{-1}, 18.1 J·kg^{-1}·K^{-1}, and 17.5 J·kg^{-1}·K^{-1} under the magnetic field in the range of 0–2 T, with the corresponding refrigerant capacity (*RC*) values of 131 J·kg^{-1}, 136 J·kg^{-1}, and 126 J·kg^{-1}, respectively. The increase of $-\Delta S_M^{max}$ for $Tm_{0.5}Er_{0.5}CuAl$ may be relevant to the change of magnetic moment distribution of Er and stress coming from element substitution. This work provides several compounds that can enrich the family of giant MCE materials in the cryogenic region.

Keywords: TmCuAl-based alloy, magnetic property, magnetocaloric effect, magnetic refrigeration

PACS: 75.30.Sg, 75.47.Np **DOI:** 10.1088/1674-1056/ac89d8

1. Introduction

Magnetocaloric effect (MCE) is a magneto-thermal transformation phenomenon in which variation of external magnetic field ($\Delta\mu_0 H$) can result in temperature change of a magnetic material.[1–3] The magnetic refrigeration based on MCE is considered to be the next-generation cryogenic refrigeration technology with great application potential. Moreover, development of materials with large MCEs is critical to achieving magnetic refrigeration applications.[4] The maximum magnetic entropy change ($-\Delta S_M^{max}$) and refrigerant capacity (*RC*) are two of the most widely used parameters for evaluating MCE of materials, and improving their values has always been the goal of efforts in the field of magnetic refrigeration.[5,6]

Over the past few decades, numerous materials with potential applications have been discovered and intensively studied in low-temperature region, including Gd_2MgTiO_6, Dy_2BaZnO_5, Sr_2GdNbO_6, $GdFe_2Si_2$, *Re*Cu*X* (*Re* = Ho, Er, and Tm; *X* = Al and Si), $ErCo_2$, $ErAl_2$, TmGa, and TmZn.[7–15] Among these compounds, *Re*CuAl (*Re* = Ho, Er, and Tm) alloys with the ZrNiAl-type hexagonal structure (space group $P\bar{6}2m$) all derive their magnetic moments from localized *Re* atoms, exhibiting giant MCEs at low field.[16] The $-\Delta S_M^{max}$ value of HoCuAl alloy is 10.3 J·kg^{-1}·K^{-1} at 12 K for a field in the range 0–1 T.[17] The neutron diffraction indicates that the magnetic moments are arranged parallel in the *ab* plane.[18] Under the field changes of 0–1 T, the $-\Delta S_M^{max}$ value of the ErCuAl compound at 7 K is 9.7 J·kg^{-1}·K^{-1}.[19] The magnetic moments of Er are determined to be parallel to the *c*-axis below the Curie temperature T_C.[20] The $-\Delta S_M^{max}$ value of TmCuAl for a field change of 0–1 T is 12.2 J·kg^{-1}·K^{-1} at 3.5 K, with the *RC* value of 44 J·kg^{-1}.[21] The neutron diffraction results reveal that the magnetic moments are along the *c*-axis in TmCuAl below $T_C = 1.9$ K, and as the temperature further decreases to 1.2 K, a rather complex magnetic structure starts to appear.[22] Comparing their $-\Delta S_M^{max}$ values, one can find that TmCuAl exhibits the largest $-\Delta S_M^{max}$ value at the field changing in 0–1 T, which is very promising for applications in the cryogenic region.

However, the theoretical magnetic moment of Tm is lower than that of the other *Re* atoms, which constrains the upper limit of MCE for the Tm-based materials. As the magnetic moments arrange along the *c*-axis in both ErCuAl and TmCuAl, the substitution of Er for Tm may be a viable option to improve the MCE. For example, Zheng *et al.* achieved an enhancement of 14.9% of the $-\Delta S_M^{max}$ by 10% Ho with a larger magnetic moment substitution for Er in ErNi.[23] In this work, $Tm_{1-x}Er_xCuAl$ ($x = 0.25$, 0.5, and 0.75) compounds were fabricated, and their structures as well as magnetic properties are systemically investigated.

2. Experimental details

The polycrystalline $Tm_{1-x}Er_xCuAl$ ($x = 0.25$, 0.5, and 0.75) alloys were fabricated by arc-melting the constituent elements (Tm and Er: purity $\geq$ 99.9 wt%; Cu and Al: purity

†Corresponding author. E-mail: mozhaojun@gia.cas.cn
‡Corresponding author. E-mail: shenbg@aphy.iphy.ac.cn

© 2022 Chinese Physical Society and IOP Publishing Ltd

$\geq$ 99.99 wt%) in an appropriate stoichiometric ratio under a high-purity argon atmosphere. To ensure homogeneity of components, the ingots were flipped and re-melted three times in the course of the melting process. The resulting ingots were sealed in evacuated quartz tubes and heat-treated at 1173 K for seven days. Subsequently, a rapid cooling process was performed by quenching in liquid nitrogen. The structure of these samples at room temperature was characterized by a Bruker D8A A25 x-ray diffractometer (XRD) with the Bragg angles 2θ in the range from 2° to 90°. Magnetic measurement was carried out by a commercial physical properties measurement system (PPMS).

3. Results and discussion

The x-ray powder diffraction patterns and Rietveld refinements for the $Tm_{1-x}Er_xCuAl$ ($x = 0.25$, 0.5, and 0.75) compounds at room temperature are shown in Figs. 1(a)–1(c). All compounds crystallize in a hexagonal ZrNiAl-type structure (space group $P\bar{6}2m$) with no impurity phase. The lattice parameters a (c) are 6.951 (3.995) Å, 6.957 (3.998) Å, and 6.963 (4.002) Å for the compounds of $x = 0.25$, 0.5, and 0.75, exhibiting a monotonous increase with the increasing Er concentration, which is attributed to the larger atom radium of Er than Tm. The crystal structure of *Re*CuAl (*Re* = Er or Tm) is plotted in Fig. 1(d). The crystal structure of *Re*CuAl consists of two types of layers, which are alternately stacked along the c-axis direction. One consists of all rare-earth atoms distributed in triangle and one third of Cu atoms. The other contains all Al atoms and the other Cu atoms. It can be inferred from the structure that this series of compounds may have strong magnetocrystalline anisotropy.

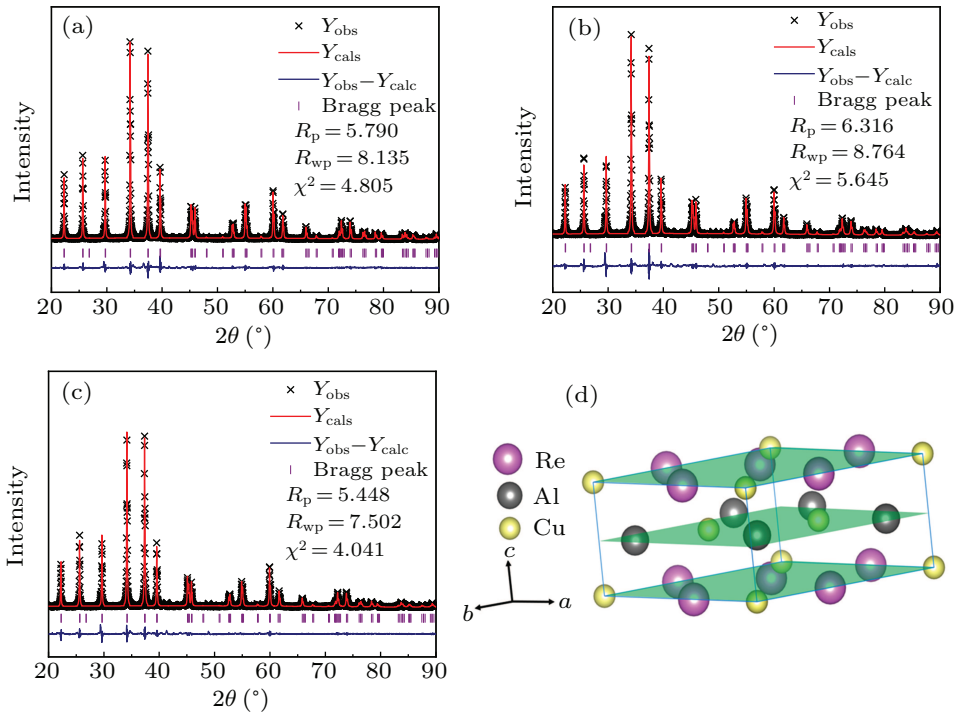


Fig. 1. The x-ray powder diffraction patterns and Rietveld refinements at room temperature for (a) $Tm_{0.75}Er_{0.25}CuAl$, (b) $Tm_{0.5}Er_{0.5}CuAl$, and (c) $Tm_{0.25}Er_{0.75}CuAl$, and (d) the crystal structure of *Re*CuAl (*Re* = Er or Tm) compound.

Figures 2(a)–2(c) displays the temperature (T) dependence of magnetization (M) under the condition of zero-field-cooling (ZFC) and field-cooling (FC) for $Tm_{1-x}Er_xCuAl$ ($x = 0.25$, 0.5, and 0.75) compounds for $\mu_0 H = 0.01$ T. These compounds show a typical ferromagnetic (FM) characteristic. A significant splitting between ZFC and FC curves is observed for these compounds at low temperature, which may be attributed to the domain-wall pining effect as usually observed in materials with low ordering temperature and high anisotropy.[24,25] Based on the ZFC curves, the dM/dT–T curves are obtained as shown in the insets. The T_C values of the compounds with $x = 0.25$, 0.5, and 0.75 are determined to be 3.2 K, 5 K, and 6 K, respectively, which correspond to the minimum values of the dM/dT–T curves.

Temperature dependences of the inverse magnetic susceptibility $1/\chi$ (symbols) and linear fitting according to the Curie–Weiss law (line) for $Tm_{1-x}Er_xCuAl$ ($x = 0.25$, 0.5, and 0.75) are shown in Fig. 2(d). The expression of the Curie–Weiss law is $\chi(T) = \frac{C}{T-\theta_P}$, where θ_P represents the paramagnetic Curie temperature, C represents the constant related to the effective magnetic moment (μ_{eff}) of lanthanide ions. It can be found that the $1/\chi$ is adequately approximated by a linear relationship and obeys the Curie–Weiss law in the

paramagnetic region. According to the fittings, the $\mu_{\rm eff}$ values are 7.6 $\mu_{\rm B}$/f.u., 8 $\mu_{\rm B}$/f.u., and 8.4 $\mu_{\rm B}$/f.u. for $x = 0.25$, 0.5, and 0.75, which are lower than their theoretical values of rare earth free ions of 8.1 $\mu_{\rm B}$/f.u., 8.6 $\mu_{\rm B}$/f.u., and 9.1 $\mu_{\rm B}$/f.u. Since the magnetic moment all originate from the *Re* atoms, the reduced magnetic moment may be related to the crystalline electric field (CEF) effects.[26,27] The values of $\theta_{\rm P}$ are 9.4 K, 8 K, and 6 K for $x = 0.25$, 0.5, and 0.75, respectively. The positive value of $\theta_{\rm P}$ also indicates that the ferromagnetic exchange interaction dominates in these compounds.

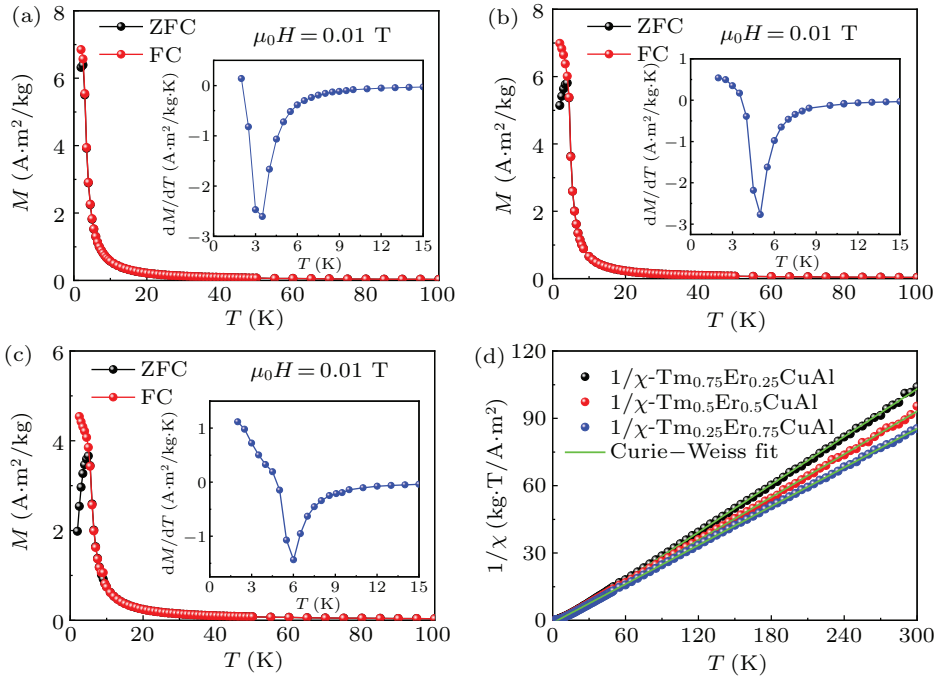


Fig. 2. Temperature dependence of magnetization measured in zero-field-cooling (ZFC) and field-cooling (FC) together with (inset) their dM/dT versus T for (a) $Tm_{0.75}Er_{0.25}CuAl$, (b) $Tm_{0.5}Er_{0.5}CuAl$, and (c) $Tm_{0.25}Er_{0.75}CuAl$ under μ_0H of 0.01 T. (d) The inverse magnetic susceptibility versus temperature (symbols) and linear fitting according to the Curie–Weiss law (line) for $Tm_{1-x}Er_xCuAl$ ($x = 0.25$, 0.5, and 0.75) under μ_0H of 0.01 T.

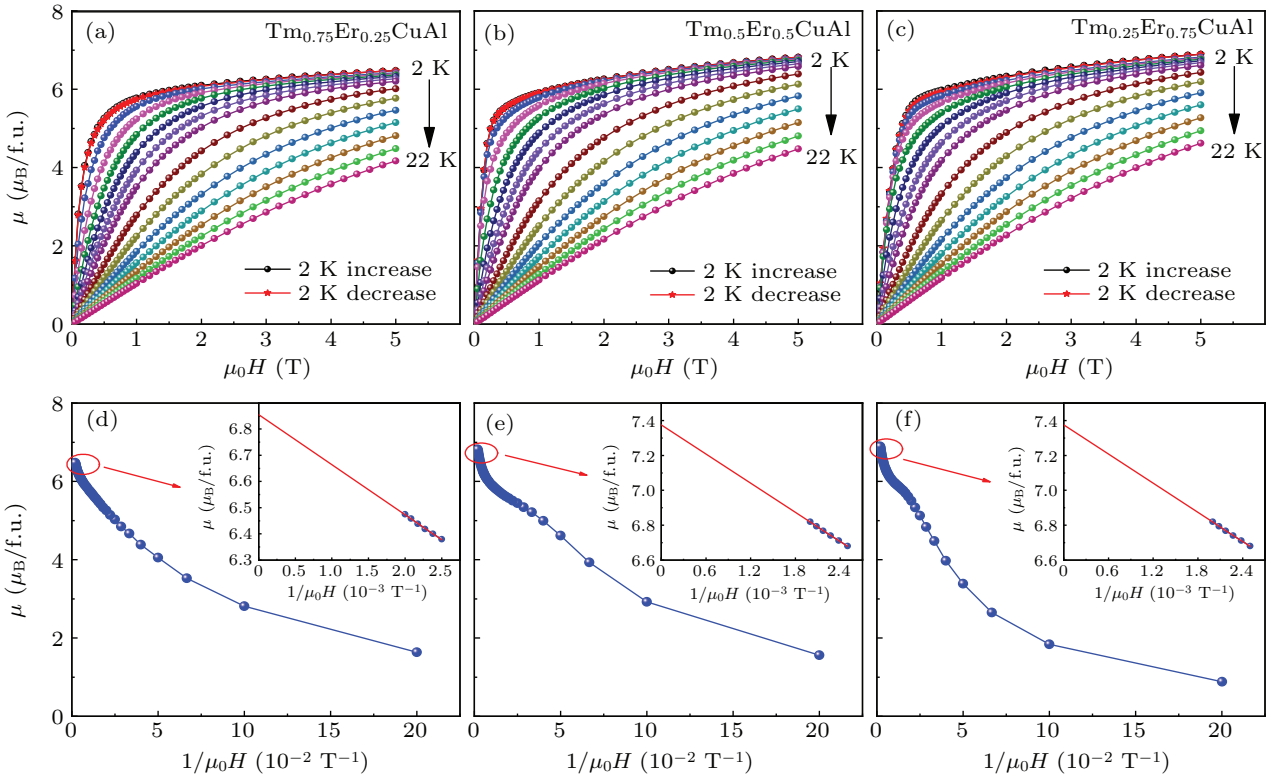


Fig. 3. (a)–(c) Isothermal magnetization curves and (d)–(f) the $1/H$ dependence of magnetization of $Tm_{1-x}Er_xCuAl$ ($x = 0.25$, 0.5, and 0.75). The insets in (d)–(f) show the μ–$1/H$ curves above the field of 4 T and their linear fitting curves.

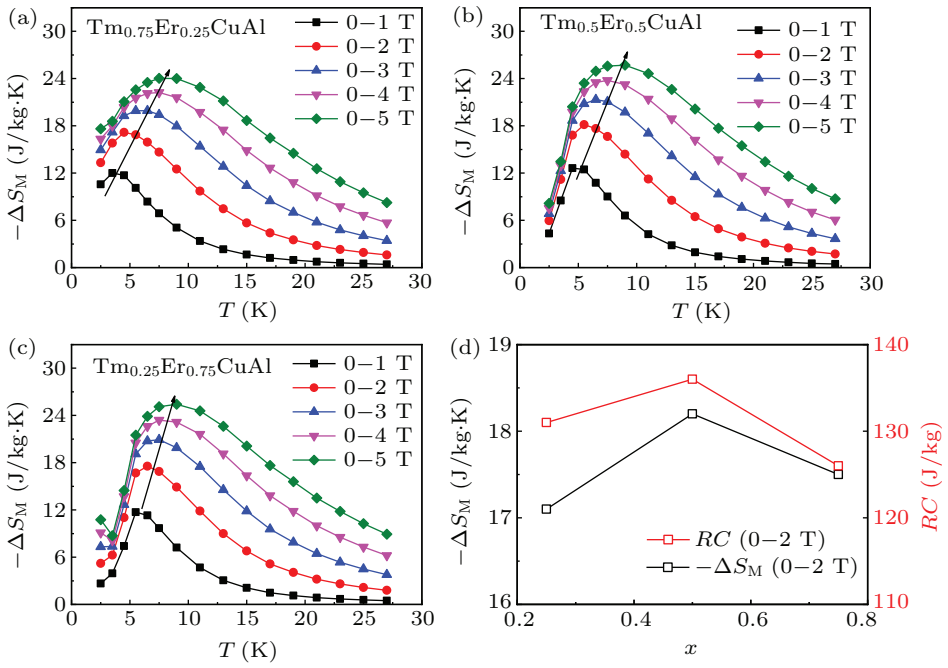


Fig. 4. The temperature dependences of $-\Delta S_M$ for (a) $Tm_{0.75}Er_{0.25}CuAl$, (b) $Tm_{0.5}Er_{0.5}CuAl$, and (c) $Tm_{0.25}Er_{0.75}CuAl$, under $\mu_0\Delta H$ from 0–1 T to 0–5 T, and (d) the $-\Delta S_M^{max}$ and RC for $x = 0.25$, 0.5, and 0.75 under $\mu_0\Delta H$ of 0–2 T.

Figures 3(a)–3(c) present the isothermal magnetization curves of $Tm_{1-x}Er_xCuAl$ ($x = 0.25$, 0.5, and 0.75) measured in a temperature region from 2 to 26 K under the applied field up to 5 T. At $T = 2$ K, the magnetization curves measured in increasing and decreasing field modes overlap completely, indicating the absence of magnetic hysteresis in these compounds. Moreover, it is observed that the magnetization of the three compounds increases rapidly with increasing magnetic field at low fields below T_C, which is a typical FM feature. As the magnetic field increases further, the magnetization starts to increase slowly and does not reach saturation until 5 T. The saturation magnetic moment (μ_s) can be evaluated by converting the μ–H curve measured at 2 K to the μ–$1/H$ curve and then extrapolating linearly the μ–$1/H$ curve in high field region to y-axis.[28] Figures 3(d)–3(f) display the μ–$1/H$ curves for compounds with $x = 0.25$, 0.5, and 0.75, where part of the μ–$1/H$ curves above the field of 4 T are selected (blue dot and line) and linearly fitted (red line) as shown in the insets. The values of μ_s are 6.85 μ_B/f.u., 7.37 μ_B/f.u., and 7.47 μ_B/f.u., for $x = 0.25$, 0.5, and 0.75, respectively, which are significantly lower than their μ_{eff} values obtained by the Curie–Weiss law. Their differences are 0.75 μ_B/f.u., 0.63 μ_B/f.u., and 0.93 μ_B/f.u., respectively. This phenomenon may be attributed to the different angles between each magnetic moment of *Re* elements and the c-axis. Although the vector sum of the magnetic moments of Tm and Er in parent-alloy is aligned parallel along the c-axis, every magnetic moment of Tm and Er has an angle with the c-axis and the angle of Tm is smaller than Er. Meanwhile, the distortion of lattice is severest for $x = 0.5$, which causes greater internal stress that may bring about a larger magnetic entropy change. It is similar to the mechanism of regulating magnetic interaction through hydrostatic pressure.[29]

Based on the Maxwell thermo-dynamic relation $\Delta S_M(T,H) = \int_0^{H_{max}} \left(\frac{\partial M}{\partial T}\right)_H dH$, magnetic entropy change (ΔS_M) could be calculated using the isothermal magnetization data, which is an essential parameter for evaluating the MCE. The $-\Delta S_M$ vs. T curves for $x = 0.25$, 0.5, and 0.75 under $\mu_0\Delta H$ from 0–1 T to 0–5 T are plotted in Figs. 4(a)–4(c). The $-\Delta S_M^{max}$ gradually increases and moves to a higher temperature with increasing $\Delta\mu_0 H$, which is a typical characteristic of the ferromagnetic property. Under the $\Delta\mu_0 H$ of 0–2 (0–5) T, the values of $-\Delta S_M^{max}$ are 17.1(24.0) J·kg^{-1}·K^{-1}, 18.1(25.7) J·kg^{-1}·K^{-1}, and 17.5(25.4) J·kg^{-1}·K^{-1} for $x =$ 0.25, 0.5, and 0.75, respectively, which are superior to the majority of alloys in the similar temperature region. In addition, there is a clear anomaly in the magnetic entropy change at low temperature under high magnetic field for the $Tm_{0.25}Er_{0.75}CuAl$ compound. This may be attributed to the presence of spin reorientation at low temperature, because every magnetic moment of Tm and Er has an angle with the c-axis and the angle of Tm is smaller than Er, which will be confirmed further in future investigation. Another crucial indicator, refrigerant capacity (RC) can also be estimated to evaluate MCE. The value of RC can be calculated by the formula $RC = \int_{T_1}^{T_2} |\Delta S_M(T)| dT$, where T_1 and T_2 are the temperatures corresponding to the $\frac{1}{2}|\Delta S_M^{max}|$, which describes the amount of heat transfer between the cold and hot reservoirs in a thermodynamic cycle. The RC values are 131(374) J·kg^{-1}, 136(377) J·kg^{-1}, and 126(364) J·kg^{-1} for $x = 0.25$, 0.5, and 0.75, respectively. In order to intuitively reflect the effect of composition change on MCE, the $-\Delta S_M^{max}$ and RC versus the

Er content x ($x = 0.25$, 0.5, and 0.75) under the $\mu_0\Delta H$ of 0–2 T are plotted in Fig. 4(d). The $-\Delta S_M^{max}$ reaches a maximum value at $x = 0.5$ and then drops with increasing x for the $\mu_0\Delta H$ of 0–2 T. The increase of MCE in $Tm_{0.5}Er_{0.5}CuAl$ is possibly due to the greatest lattice distortion within the compound system resulting in greater internal stresses, which brings about a larger $-\Delta S_M^{max}$, similar to hydrostatic pressure, as in HoCuSi.[29] The increase in μ_s with increasing Er content is attributed to the larger magnetic moment of Er than Tm.

The nature of magnetic phase transition of $Tm_{1-x}Er_xCuAl$ ($x = 0.25$, 0.5, and 0.75) can also be determined by a phenomenological procedure presented by Franco *et al.*[30] According to the procedure, the normalized magnetic entropy change ($\Delta S'$) as a function of the rescaled temperature (θ) is obtained by the reconstruction of the $-\Delta S_M$ vs. T curves under various $\Delta\mu_0 H$. The $\Delta S'$ is defined as $\Delta S_M(T)/\Delta S_M^{max}$, while the θ is rescaled by a different way below and above T_C expressed as follows:

$$\theta = \begin{cases} -(T - T_C)/(T_{r1} - T_C), & T \le T_C, \\ (T - T_C)/(T_{r2} - T_C), & T > T_C, \end{cases}$$

where T_{r1} and T_{r2} are the two reference temperatures corresponding to $0.6 \times |\Delta S_M^{max}|$ and $T_{r1} < T_{r2}$. When $T_{r1} < 2.5$ K, the T_{r1} value is approximately estimated by extending the endpoints of $-\Delta S_M$ vs. T curves to the point (0, 0).

The rebuilt $\Delta S'$–θ curves of $Tm_{1-x}Er_xCuAl$ ($x = 0.25$, 0.5, and 0.75) are given in Fig. 5. For compounds with $x = 0.5$, and 0.75, the $\Delta S'$–θ curves at $\mu_0\Delta H$ of 0–1 T do not completely overlap with the other curves for $\theta < 0$, which is caused by taking too few points at $\theta < 0$. The rest of the $\Delta S'$–θ curves almost collapse on the same universal curve at different magnetic fields, proving their second-order phase transition nature.

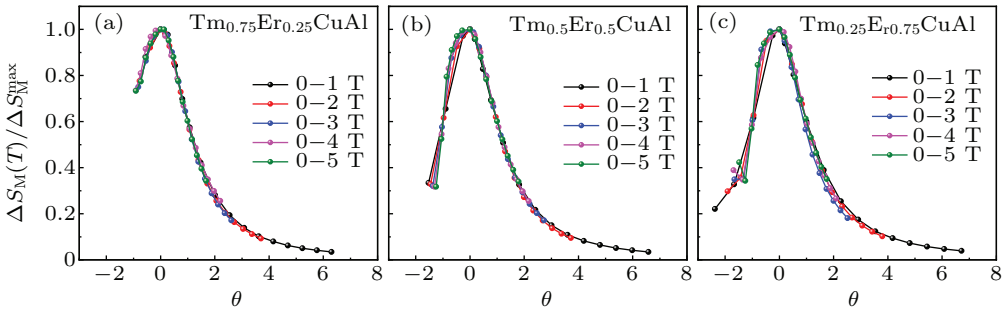


Fig. 5. Normalized magnetic entropy change as a function of the rescaled temperature for (a) $Tm_{0.75}Er_{0.25}CuAl$, (b) $Tm_{0.5}Er_{0.5}CuAl$, and (c) $Tm_{0.25}Er_{0.75}CuAl$, under $\mu_0\Delta H$ from 0–1 T to 0–5 T.

4. Conclusion

In summary, we have prepared $Tm_{1-x}Er_xCuAl$ ($x = 0.25$, 0.5, and 0.75) alloys by arc-melting, and investigated their structural and magnetic properties. All compounds undergo a second-order phase transition transition from FM to PM at the corresponding T_C of 3.2 K, 5 K, and 6 K for the compounds with $x = 0.25$, 0.5, and 0.75, respectively. Under the field change of 0–2 (5) T, the values of $-\Delta S_M^{max}$ are 17.1(24.) J·kg^{-1}·K^{-1}, 18.1(25.7) J·kg^{-1}·K^{-1}, and 17.5(25.4) J·kg^{-1}·K^{-1} for $x = 0.25$, 0.5, and 0.75, with the corresponding *RC* values of 131(374) J·kg^{-1}, 136(377) J·kg^{-1}, and 126(364) J·kg^{-1}, respectively. The best performance of the $Tm_{0.5}Er_{0.5}CuAl$ compound may come from the increase in μ_s with increasing Er content that is attributed to larger magnetic moment of Er than Tm, and the greatest lattice distortion within the compound system results in greater internal stresses, which brings about a larger $-\Delta S_M^{max}$ similar to hydrostatic pressure. The outstanding MCE and no hysteresis behavior of $Tm_{1-x}Er_xCuAl$ ($x = 0.25$, 0.5, and 0.75) make them very attractive in low temperature region.

Acknowledgements

Project supported by the National Natural Science Foundation of China (Grant Nos. 52171195, and 52171054), the National Science Foundation for Distinguished Young Scholars (Grant No. 51925605), and the Scientific Instrument Developing Project of Chinese Academy of Sciences (Grant No. YJKYYQ20200042).

References

[1] Zhang H, Li Y W, Liu E K, Ke Y J, Jin J L, Long Y and Shen B G 2015 *Sci. Rep.* **5** 11929
[2] Kimel A V, Kirilyuk A, Tsvetkov, Pisarev R V and Rasing T 2004 *Nature* **429** 850
[3] Pecharsky V K and Gschneidner K A 1997 *Appl. Phys. Lett.* **70** 3299
[4] Chen D, Taylor K P, Hall Q and Kaplan J M 2016 *Genetics* **204** 1151
[5] Zhang Z Y, Tang Q, Wang F C, Zhang H Y, Zhou Y X, Xia A L, Li H L, Chen S S and Li W H 2019 *Intermetallics* **111** 106500
[6] Dong X S, Feng J, Yi Y L and Li L W 2018 *J. Appl. Phys.* **124** 093901
[7] Zhang Y K. Tian Y, Zhang Z Q, Jia Y S, Zhang B, Jiang M Q, Wang J and Ren Z M 2022 *Acta Mater.* **226** 117669
[8] Xu P, Hu L, Zhang Z Q, Wang H F and Li L W 2022 *Acta Mater.* **236** 118114
[9] Xu P, Ma Z P, Wang P F, Wang H F and Li L W 2021 *Mater. Today Phys.* **20** 100470
[10] Zhang Y K, Zhu J, Li S, Zhang Z Q, Wang J and Ren Z M 2022 *Sci. China Mater.* **65** 1345
[11] Zhang H and Shen B G 2015 *Chin. Phys. B* **24** 127504

[12] Giguere A, Foldeaki M, Schnelle W and Gmelin E 1999 *J. Phys.: Condens. Matter.* **11** 6969

[13] Pecharsky V K and Gschneidner K A 1998 *Phys. Rev. B* **58** 12110

[14] Mo Z J, Shen J, Yan L Q, Tang C C, Lin J, Wu J F, Sun J R, Wang L C, Zheng X Q and Shen B G 2013 *Appl. Phys. Lett.* **103** 052409

[15] Li L W, Yuan Y, Zhang Y K, Namiki T, Nihimura K, Pöttgen R and Zhou S Q 2015 *Appl. Phys. Lett.* **107** 132401

[16] Gupta S and Suresh K G 2015 *J. Alloys Compd.* **618** 562

[17] Wang L C, Dong Q Y, Mo Z J, Xu Z Y, Hu F X, Sun J R and Shen B G 2013 *J. Appl. Phys.* **114** 163915

[18] Oesterreicher H 1973 *J. Less Common Met.* **30** 225

[19] Dong Q Y, Chen J, Shen J, Sun J R and Shen B G 2012 *J. Magn. Magn. Mater.* **324** 2676

[20] Javorský P, Burlet P, Ressouche E, Sechovský V, Michor H and Lapertot G 1996 *Physica B* **225** 230

[21] Mo Z J, Shen J, Yan L Q, Wu J F and Wang L C 2013 *Appl. Phys. Lett.* **102** 192407

[22] Javorsky P, Gubbens P C M, Mulders A M, Prokeš K, Stüsser N, Gortenmulder T J and Hendrikx R W A 2002 *J. Magn. Magn. Mater.* **251** 123

[23] Zheng X Q, Zhang B, Wu H, Hu F X, Huang Q Z and Shen B G 2016 *J. Appl. Phys.* **120** 163907

[24] Zhang H, Shen B G, Xu Z Y, Shen J, Hu F X, Sun J R and Long Y 2013 *Appl. Phys. Lett.* **102** 092401

[25] Wang J L, Marquina C, Ibarra M R and Wu G H 2006 *Phys. Rev. B* **73** 094436

[26] Farrell J and Wallace W E 1966 *J. Inorg. Chem.* **5** 105

[27] Gignoux D and Givord F 1983 *J. Magn. Magn. Mater.* **31** 217

[28] Ćwik J, Koshkid'ko Y, Nenkov K, Tereshina-Chitrova E and Kolchugina N 2021 *J. Alloys Compd.* **859** 157870

[29] Hao J Z, Hu F X, Zhou H B, Liang W H, Yu Z B, Shen F R, Gao Y H, Qiao K M, Li J, Zhang C, Wang B J, Wang J, He J, Sun J R and Shen B G 2020 *Scr. Mater.* **186** 84

[30] Franco V and Conde A 2010 *Int. J. Refrig.* **33** 465